

Developing AlMn films for Argonne TES fabrication

E.M. Vavagiakis¹, N.F. Cothard², J.R. Stevens¹,
C.L. Chang³, M.D. Niemack¹, G. Wang³, V.G.
Yefremenko³, J. Zhang³

the date of receipt and acceptance should be inserted later

Abstract The reference design for the next-generation cosmic microwave background (CMB) experiment, CMB-S4, relies on large arrays of transition edge sensor (TES) bolometers coupled to Superconducting Quantum Interference Device (SQUID)-based readout systems. Mapping the CMB to near cosmic variance limits will enable the search for signatures of inflation and constrain dark energy and neutrino physics. AlMn TESes provide simple film manufacturing and highly uniform arrays over large areas to meet the requirements of the CMB-S4 experiment. TES parameters such as critical temperature and normal resistance must be tuned to experiment specifications and can be varied based on geometry and steps in the fabrication process such as deposition layering, geometry, and baking time and temperature. Using four-terminal sensing, we measured T_C and R_N of AlMn 2000 ppm films and devices of varying thicknesses fabricated at Argonne National Laboratory to motivate device geometries and fabrication processes to tune T_C to 150-200 mK and R_N to ~ 10 mOhms. Measurements of IV curves and time constants for the resulting devices of varying leg length were made using time-division SQUID multiplexing, and determined T_C , G , k , f_{3db} , and R_N . We present the results of these tests along with the geometries and fabrication steps used to tune the device parameters to the desired limits.

Keywords Superconducting detectors, Transition edge sensors, Bolometers, Nanofabrication

1 Introduction

The cosmic microwave background (CMB) contains a wealth of information about the origins, evolution, and fundamental physics of our universe. CMB-S4 is a proposed “Stage-4” ground-based CMB experiment that will map the polarization of the CMB in multiple frequency bands to nearly the cosmic variance limit. CMB-S4 targets science goals that include characterizing dark energy and dark matter, searching for signatures of inflation in the early

¹Department of Physics, Cornell University, Ithaca, NY 14853, USA

²Department of Applied Physics, Cornell University, Ithaca, NY 14853, USA

³Argonne National laboratory, 9700 S Cass Ave, Lemont, IL 60439, USA

Tel.: (607) 255-0474

E-mail: ev66@cornell.edu

universe, measuring the sum of the neutrino masses, and mapping the universe's matter distribution [1].

CMB-S4 will rely on large arrays of Transition-Edge Sensors (TESes) coupled to Superconducting Quantum Interference Device (SQUID)-based readout systems to reach its sensitivity targets [2, 3]. TESes are a mature technology and have been thoroughly demonstrated to achieve CMB science goals. TESes are also scalable, enabling the order of magnitude higher detector counts required by CMB-S4. The choice of AlMn TESes will provide CMB-S4 with simple film manufacturing and highly uniform distributions of device parameters over large arrays [4, 5].

Monolithic arrays of multichroic TESes have been previously fabricated at Argonne National Laboratory and deployed in the South Pole Telescope's SPT-3G camera [6]. These Ti/Au bolometers have a critical temperature of $T_C = 420$ mK and a normal resistance of $R_N = 2 \Omega$. To meet the experiment design requirements for CMB-S4, AlMn_{2000ppm} TES fabrication will target a $T_C \sim 150$ -200 mK and an $R_N \sim 10$ -20 m Ω . While SPT-3G used a ^4He - ^3He - ^3He absorption refrigerator with a bath temperature of ~ 250 mK, CMB-S4 will use dilution refrigerators with bath temperatures < 100 mK [7]. Reducing the bath temperature will reduce the thermal fluctuation noise. Reducing R_N will optimize the detector arrays for TDM or microwave-SQUID multiplexing (μMUX) readout. The fabrication process at Argonne will therefore need to be tuned to achieve these device parameters. Variables in the fabrication process such as the Mn concentration, thickness and geometry of films, thermal annealing temperature, and presence of additional material layers all affect the AlMn device parameters and must be tuned to meet specifications through repeated rounds of fabrication and testing [4, 8].

2 Fabrication

Film samples and devices were fabricated at Argonne National Laboratory and tested at Cornell University to develop the fabrication process. Bare film studies were performed to study the impact of substrate choice and Ti (or Mo) buffer layer between AlMn and Au depositions. A film stack of 2000ppm AlMn on SiO₂ with a Ti15nm/Au15nm top layer was chosen based on good critical temperature repeatability and was derived from the Ti/Au SPT-3G array fabrication (Fig. 1). The top layer of Au was chosen to prevent oxidation and protect the underlying films, while remaining conductive to connect leads to the device. Patterned films were then tested to predict device T_C and R_N .

The thickness and aspect ratio of the film stacks was then iterated upon to target the desired R_N . Baking time and temperature were selected to target T_C . A lift-off process is used for TES patterns, which can potentially lead to tapered edges and interaction between the Al and Au layers, and thus to poor transitions for thicker films. Furthermore, direct contact of Al and Au leads to the formation of intermetallic compounds and the variation of superconducting properties. Such effects as well as proximity effects were considered while iterating on patterned films and TESes.

3 Testing

Film samples, patterned films, and TESes from Argonne were tested at Argonne and Cornell University.

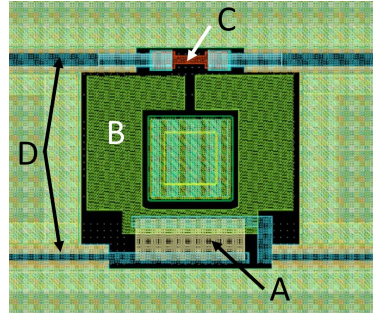


Fig. 1 A modified SPT-3G TES island, where (A) is the AlMn TES film, (B) is Pd for heat capacity stabilization, (C) is a load resistor, and (D) are the Nb leads. The AlMn200nm/Ti15nm/Au15nm TES film is 15 μm long by 80 μm wide.

3.1 Four-lead measurements

Samples were wire bonded and affixed with rubber cement to a printed circuit board (PCB) and mounted to the coldest (100 mK) stage of a dilution refrigerator with an internal 300 K magnetic shield. Four-lead measurements were taken of the samples, which precisely measure low resistance values by eliminating the lead and contact resistances from the measurements. Temperature was varied as resistances were logged via a Lakeshore AC resistance bridge, reading out the superconducting transition and measuring T_C and R_N . For each transition, T_C was taken to be the temperature value at 50% R_N , where R_N is the resistance value measured at 2 mK above the last superconducting data point in the resistance versus temperature curve (Fig. 2). Excitation currents were varied to ensure their choice didn't significantly affect the measured T_C . Based on the noise in the obtained curves due to temperature fluctuations and Lakeshore measurements, the total uncertainty on T_C is taken to be 2 mK, and the uncertainty on R_N to be 0.2 m Ω .

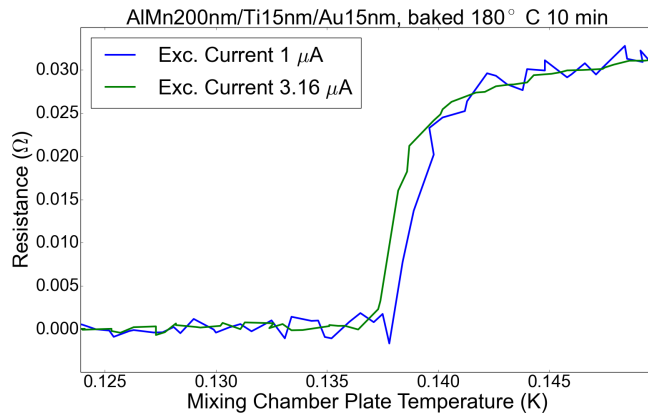


Fig. 2 Example of the four-lead R vs. T measurement of a film superconducting transition. Choice of excitation current influences results, and T_C is recorded for an excitation current which has been reduced enough to keep T_C consistent within 2 mK.

3.2 TDM SQUID readout measurements

Fabricated TESes of two different leg lengths (865 μm and 446 μm) of equal cross-sectional area (21 μm wide, 1 μm SiN + 0.3 μm Nb + 0.5 μm SIO2 thick), were mounted to a PCB on the cold stage of the dilution refrigerator, and read out using the same time division multiplexing (TDM) system used in AdvACT with NIST SQUIDs [9]. TDM measurements of current-voltage (IV) curves at various bath temperatures were acquired for a “long” and “short” leg length AlMn_{2000ppm}200nm/Ti15nm/Au15nm TES. We define P_{sat} to be the bias power which drives the TES to 90% of its normal resistance, R_N . The measured P_{sat} values are fit to the model

$$P_{sat} = K(T_C^n - T_{bath}^n), \quad (1)$$

where P_{sat} is related to the bath temperature T_{bath} and the critical temperature (T_C) of the device. Because K is degenerate with n in our fits, we hold n fixed at a range of values while fitting the other parameters, and finally determine the best fit n by plotting n vs χ^2 and obtaining the minimum χ^2 . The thermal conductivity, G , of the device is then given by

$$G = \frac{dP_{sat}}{dT_C} = nKT_C^{n-1}. \quad (2)$$

The temporal response of a given TES can be defined in terms of $f_{3dB} = 1/2\pi\tau_{eff}$, where τ_{eff} is the effective time thermal constant of the TES operated under negative electrothermal feedback. To measure f_{3dB} , a small amplitude square wave is added to the DC detector voltage bias. The detector response is sampled quickly at ~ 1600 Hz. The time constant, τ_{eff} , is extracted by fitting the response to a single pole exponential. These measurements are performed at multiple bath temperatures and at several different points on the superconducting transition [10]. As a next step, we are working on noise data acquisitions for Argonne TESes [11].

4 Results

4.1 Four-lead measurement results

The critical temperature and normal resistance measurements for TESes and films varying in material, geometry, and bake time and temperature are given in Table 1. Baking was found to shift T_C , and the films showed evidence of annealing, where T_C doesn't change again after the first bake. Thicker and wider geometries lowered R_N to approach the target value, and aspect ratios were also found to influence T_C (Fig. 3).

4.2 TDM measurement results

The results of P_{sat} fits (Fig. 4) for two Argonne devices are shown in Table 2. The results of bias step measurements are shown in Fig. 5. We observe a large decrease in time constant as the detectors are biased lower on the superconducting transition, which is consistent with previous AlMn TES measurements [10].

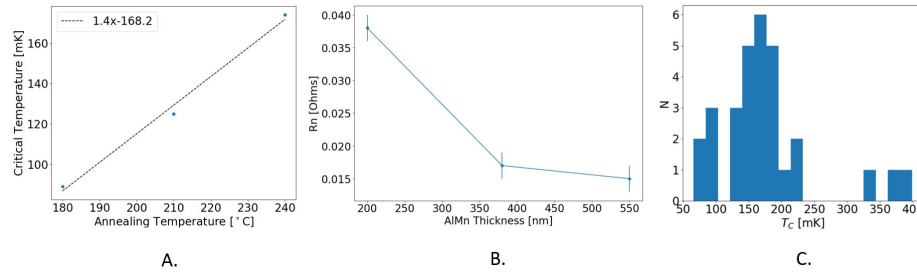


Fig. 3 A: Critical temperature vs. annealing temperature for three AlMn_{2000ppm}200nm/Ti15nm/Au15nm films along with linear fit showing the effect of baking on T_C . B: Normal resistance vs. AlMn thickness in nm for three film samples, showing R_N decreasing with increasing material thickness. C: Histogram of all Argonne sample critical temperatures measured at Cornell, highlighting a trend of narrowing in on the desired critical temperature of 150-200 mK for CMB-S4.

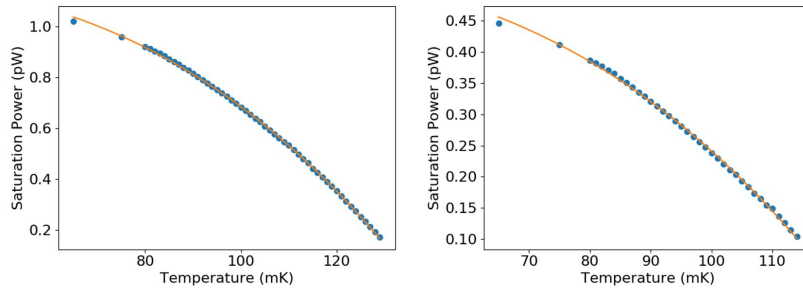


Fig. 4 Saturation power versus temperature along with fits to P_{sat} measurements for two devices. *Left*: Argonne short leg length (446 μm) TES. *Right*: Argonne long leg length (865 μm) TES. The best fit n values for these data were 2.76 and 2.91 for the short and long leg lengths respectively.

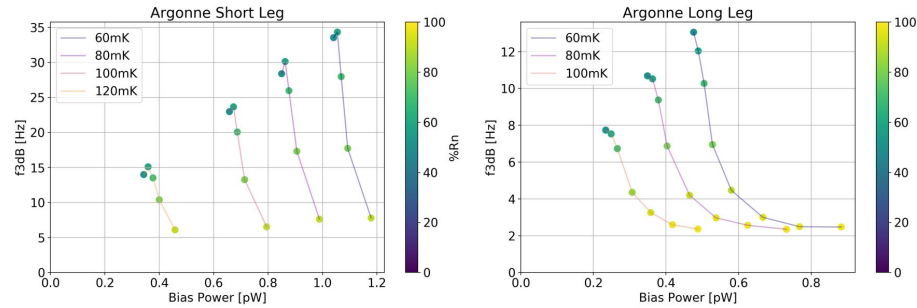


Fig. 5 Results of bias step measurements. f_{3dB} versus bias power in pW for four bath temperatures. *Left*: Argonne short leg length (446 μm) TES. *Right*: Argonne long leg length (865 μm) TES.

Film	Heating °C	T_C [mK]	R_N [Ω]
Ti5nm/AlMn _{1200ppm} 100nm/Ti5nm/Au20nm	0	196	0.86
Ti5nm/AlMn _{1200ppm} 100nm/Ti5nm/Au20nm	180/10 min	153	0.80
Ti5nm/AlMn _{1200ppm} 100nm/Ti5nm/Au20nm	180/10 min, 90/2 min, 110/2 min	141	0.77
AlMn _{1200ppm} 100nm/Mo10nm/Au20nm	0	371	0.27
AlMn _{1200ppm} 100nm/Mo10nm/Au20nm	180/10 min	399	0.37
AlMn _{2000ppm} 100nm/Ti15nm/Au15nm	0	223	0.43
AlMn _{2000ppm} 100nm/Ti15nm/Au15nm	0	159	1.65
AlMn _{2000ppm} 100nm/Ti15nm/Au15nm	180/10 min	181	1.45
AlMn _{2000ppm} 100nm/Ti15nm/Au15nm	180/10 min, 90/2 min, 110/1.5 min	180	1.46
AlMn _{2000ppm} 100nm/Ti15nm/Au15nm	0	179	0.09
AlMn _{2000ppm} 100nm/Ti15nm/Au15nm	180/10 min	193	0.05
AlMn _{2000ppm} 100nm/Ti15nm/Au15nm	180/10 min, 90/2 min, 110/1.5 min	172	0.05
AlMn _{2000ppm} 100nm/Ti15nm/Au15nm	0	167	3.31
AlMn _{2000ppm} 100nm/Ti15nm/Au15nm	180/10 min	160	3.06
AlMn _{2000ppm} 80nm	0	335	2.10
AlMn _{2000ppm} 550nm/Ti15nm/Au15nm	0	151	0.22
AlMn _{2000ppm} 550nm/Ti15nm/Au15nm	0	146	0.11
AlMn _{2000ppm} 550nm/Ti15nm/Au15nm	180/10 min	66	0.11
AlMn _{2000ppm} 550nm/Ti15nm/Au15nm	180/20 min	67	0.11
AlMn _{2000ppm} 200nm/Ti15nm/Au15nm*	0	127	0.03
AlMn _{2000ppm} 200nm/Ti15nm/Au15nm*	180/10 min	129	0.04
AlMn _{2000ppm} 200nm/Ti15nm/Au15nm*	180/10 min	140	0.04
AlMn _{2000ppm} 380nm/Ti15nm/Au15nm*	180/10 min	179	0.02
AlMn _{2000ppm} 550nm/Ti15nm/Au15nm*	180/10 min	167	0.02
AlMn _{2000ppm} 550nm/Ti15nm/Au15nm*	0	219	0.02
AlMn _{2000ppm} 550nm/Ti15nm/Au15nm*	180/20 sec + 10 min	88	0.01
AlMn _{2000ppm} 550nm/Ti15nm/Au15nm*	180/60 sec + 10 min	86	0.01
AlMn _{2000ppm} 200nm/Ti15nm/Au15nm	180	89	0.03
AlMn _{2000ppm} 200nm/Ti15nm/Au15nm	210	125	0.03
AlMn _{2000ppm} 200nm/Ti15nm/Au15nm	240	174	0.03
Film	Length [μ m] x Width [μ m]	T_C	R_N
AlMn _{2000ppm} 200nm/Ti15nm/Au15nm	5x80	201	0.01
AlMn _{2000ppm} 200nm/Ti15nm/Au15nm	20x200	126	0.01
AlMn _{2000ppm} 200nm/Ti15nm/Au15nm	5x140	172	0.01
AlMn _{2000ppm} 200nm/Ti15nm/Au15nm	10x200	146	0.01

Table 1 Samples tested using four-lead measurements, with various materials, geometries, bake times and temperatures, and resulting critical temperatures and normal resistances. *=TES devices.

Parameter	Leg Length 865 μ m Fit	Leg Length 446 μ m Fit
T_C	122 mK	136 mK
G	0.013 pW/mK	0.024 pW/mK
k	4.6e-7 pW/mK ⁿ	1.5e-6 pW/mK ⁿ
R_N	21.9 m Ω	21.7 m Ω

Table 2 Parameter fits to P_{sat} measurements from Fig. 4, Eqs. 1, 2, for two Argonne devices of different leg length and identical leg cross-sectional area. The best fit values for these data were $n = 2.76$ and $n = 2.91$ for the short and long leg lengths respectively.

5 Summary

We have measured T_C , G , k , f_{3db} , and R_N for two Argonne AlMn TESes, and T_C and R_N for various film stacks to motivate the selection of materials, thickness, geometry, and bake time and temperature. Through iterative testing, we inform Argonne's fabrication process to produce TESes which have the desired critical temperature (150-200 mK) and normal resistance (10-20 m Ω) to be used for precision measurements of the CMB in the next-generation

CMB experiment, CMB-S4. Next steps will include fabrication of devices with higher saturation powers (2 pW-20 pW) and lower time constants (0.3-3 ms) to optimize the TES performance for all the CMB-S4 frequency bands.

Acknowledgements Work at Argonne, including use of the Center for Nanoscale Materials, an Office of Science user facility, was supported by the U.S. Department of Energy, Office of Science, Office of Basic Energy Sciences and Office of High Energy Physics, under Contract No. DE-AC02-06CH11357. This material is based upon work supported by the National Science Foundation Graduate Research Fellowship Program under Grant No. DGE-1650441 (EMV) and NSF CAREER award No. 1454881 (MDN). Work by NFC was supported by a NASA Space Technology Research Fellowship.

References

1. K. N. Abazajian, et al., CMB-S4 Science Book, First Edition, 2016, arXiv:1610.02743.
2. M. H. Abitbol, et al., CMB-S4 Technology Book, First Edition, 2017, arXiv:1706.02464.
3. K.N. Abazajian et al., CMB-S4 Science Case, Reference Design, and Project Plan, 2019, arXiv:1907.04473
4. D. Li et al., AlMn Transition Edge Sensors for Advanced ACTPol, J Low Temp Phys (2016) 184: 66. <https://doi.org/10.1007/s10909-016-1526-8>
5. Shuay-Pwu Patty Ho et al., Highly uniform 150 mm diameter multichroic polarimeter array deployed for CMB detection, Proc. SPIE 9914 (2017), Millimeter, Submillimeter, and Far-Infrared Detectors and Instrumentation for Astronomy VIII, 991418.
6. Posada, C. M., et al. (2015). Fabrication of large dual-polarized multichroic TES bolometer arrays for CMB measurements with the SPT-3G camera. Superconductor Science and Technology, 28(9), [094002]. DOI:10.1088/0953-2048/28/9/094002
7. J. A. Sobrin et al. (2018). Design and characterization of the SPT-3G receiver, Proc. SPIE 10708, DOI:10.1117/12.2314366
8. D. R. Schmidt, H. M. Cho, et al., Al-Mn Transition Edge Sensors for Cosmic Microwave Background Polarimeters, App. Superconductivity (2011), IEEE Transactions on 21 (3), 196-198, doi:10.1109/TASC.2010.2090313.
9. S. W. Henderson et al., Proc. SPIE 9914, 99141G (2016), DOI:10.1117/12.2233895
10. B.J. Koopman et al., J. Low Temp. Phys. (2018), doi:10.1007/s10909-018-1957-5
11. J.R. Stevens, N.F. Cothard, E.M. Vavagiakis, et al., J. Low Temp. Phys. This Special Issue (2019).